Publications of the Korean Astronomical Society
**27**: 253 ∼ 256, 2012 September

ISSN 1225-1534 (Print)
http://dx.doi.org/10.5303/PKAS.2012.27.4.253

# INTERSTELLAR DUST IN M51 FROM IRC IMAGES

Fumi Egusa[1], I. Sakon[2], T. Onaka[2], H. Matsuhara[1], K. Arimatsu[1,2],
T. Suzuki[1], T. Wada[1], and the IRC team
[1]Institute of Space and Astronautical Science, Japan Aerospace Exploration Agency, Kanagawa 252-5210, Japan
[2]Graduate School of Science, The University of Tokyo, Tokyo 113-0033, Japan
*E-mail: fegusa@ir.isas.jaxa.jp*
*(Received July 01, 2012; Accepted August 03, 2012)*

## ABSTRACT

We present the IRC images of M51, a pair of interacting galaxies. Given the high angular resolution (7.4″) and the wide field of view (∼ 10′) covering almost the entire M51 system, we investigate dust properties and their connection to the spiral arm structure. We have applied image-filtering processes including the wavelet analysis to the N3 image, which traces the total stellar mass best among the IRC bands. From this filtered image, the center, arm, and interarm regions are defined. A color, or flux ratio among the MIR bands, has been measured at each pixel (3.7″ in size). We find a wide variety of S7/S11 with a difference between arm and interarm regions. We also find that at some positions S11 seems to be higher than predicted by MW dust models. Estimated contributions from the stellar continuum and gas emission lines to the band are not enough to explain this discrepancy. From these results, we deduce that the PAH ionization condition and its fraction to the total dust mass in M51 are different from those in MW.

*Key words:* galaxies: individual (M51); galaxies: spiral; ISM: dust

## 1. INTRODUCTION

Interstellar dust is abundant and widely distributed especially within disks of late-type galaxies. Since the properties of dust reflect conditions of its environments, emission from dust is an important probe for the interstellar medium. Dust around star forming regions absorbs intense star light and radiates the absorbed energy in the infrared (IR) regime. As well as continuum emission, many spectral band features are observed at near- to mid-IR wavelengths, and polycyclic aromatic hydrocarbons (PAHs) have been regarded to be their major carriers.

The Infrared Camera (IRC; Onaka et al., 2007) onboard the AKARI satellite (Murakami et al., 2007) has a wide field of view of ∼ 10′. In addition, three channels, NIR, MIR-S, and MIR-L, and three bands in each channel cover the wavelength range of 2–25 $\mu$m continuously. These bands efficiently trace the interstellar dust in different conditions, helping us to reveal dust properties comprehensively. The angular resolution is 4.0″–6.8″, high enough to investigate galactic structures in nearby galaxies.

In this study, we present AKARI MIR images of M51, a pair of the grand-design spiral galaxy, M51a (NGC 5194) and the companion galaxy, M51b (NGC 5195). With the wide field of view, multiple photometric bands, and high angular resolution, we are able to examine the interstellar dust condition in detail and its relationship to the spiral structure. At an adopted distance of 8.4 Mpc to M51 (Feldmeier et al., 1997), 1″ corresponds to 41 pc.

## 2. DATA REDUCTION

The IRC data sets used in this work were taken during two pointed observations as a part of the mission program, "ISM in our Galaxy and Nearby Galaxies"

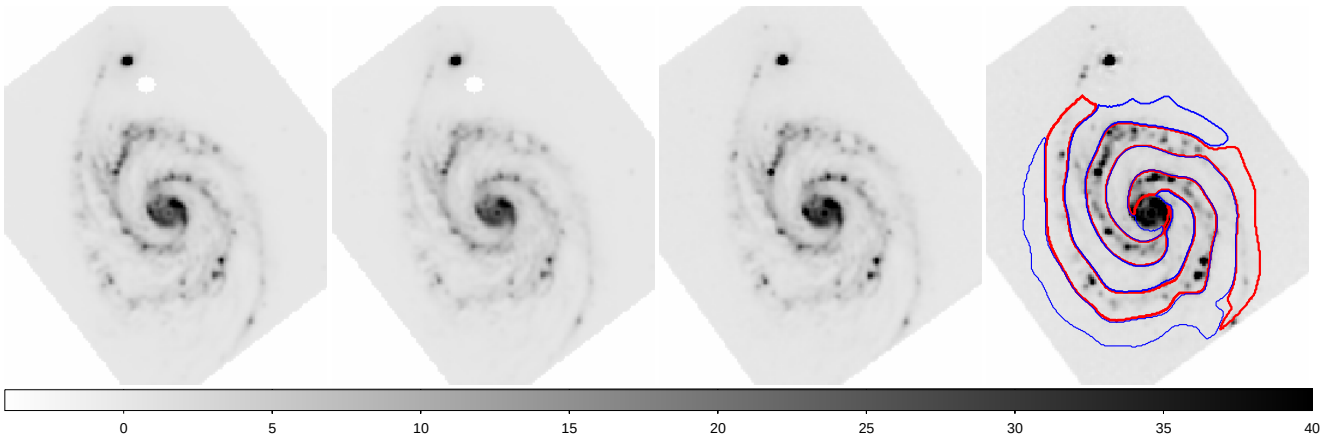


**Fig. 1.** Fully reduced and calibrated images of S7, S11, L15, and L24 (from left to right) for M51. The unit for gray scale is MJy/sr. In the right panel, the defined arm and interarm regions are indicated by red and blue lines, respectively.

(ISMGN; Kaneda et al., 2009).

In the following parts of this section, we briefly describe reduction procedures which are not included in the standard pipeline of the IRC imaging toolkit[1] but are necessary for the M51 data. Fully reduced and calibrated MIR images are presented in Figure 2..

### 2.1. *Neighbor Dark Frames*

Since the observations on orbit started, the number of hot and warm pixels has increased with time, especially in the MIR-L channel. Two types of dark frames provided by the pipeline have a disadvantage: a super dark is not best suited to data taken at later stages while a self dark is created only from a few frames. We thus created a new set of dark frames called neighbor dark. In order to decrease the statistical uncertainty (than self dark) and to better calibrate temporal variations (than super dark), we combined all pre-dark frames taken within a certain period of time to construct neighbor dark frames.

### 2.2. *Earthshine Light Removal*

The background of MIR-L images of M51 was found to be contaminated by the Earthshine Light (EL). Since the EL pattern is extended and difficult to be separated from the object, M51, we used other data sets taken under similar conditions (i.e. date and target coordinates) but without any diffuse sources and created an EL pattern for each of L15 and L24.

[1] available from http://www.ir.isas.jaxa.jp/ASTRO-F/Observation/.

Scripts for making and subtracting the EL pattern are now included in the IRC toolkit as `mk_el.cl` and `sub_el.cl`, respectively.

### 2.3. *PSF Correction*

In order to investigate brightness ratios between different bands, we applied the Point Spread Function (PSF) correction to the four MIR images, using the Fast Fourier Transform and PSF patterns provided by Arimatsu et al. (2011). The corrected PSF is a 2D Gaussian with full width at half maximum (FWHM) of 7.4″, which corresponds to $\sim$ 300 pc. A pixel size is 3.7″ on a side.

### 2.4. *Ghost Masking*

A bright compact object close to M51b in the southwest direction, which is apparent only in MIR-S images, was found to be an artifact called ghost of this companion galaxy, arising from internal reflection in the beam splitter. The relative peak flux of the ghost to M51b is larger at S11 than S7.

Arimatsu et al. (2011) provided template patterns of artifact features for each band. However, we found that their ghost template is not applicable to our data sets. It is plausibly due to a combination of (1) the location of M51b, which is close to the detector edge while the template is created for the source at the middle, (2) the ghost amplitude dependence on the source color, (3) the brightness of M51b, which is close to the saturation limit.

We therefore decided to mask a circular area with radius of 15″ around the ghost peak defined in the S11

image.

## 3. ARM DEFINITION

In this study, we basically followed the procedures of Dumas et al. (2011), who applied the wavelet analysis to the 20 cm radio continuum image of M51 to separate arm and interarm regions. Among the IRC bands of M51, N3 with the shortest observing wavelength, is thought to best trace the stellar mass, i.e. gravitational potential of the disk. The 2MASS $K_s$-band image (Jarrett et al., 2003), which is widely used as a tracer of stellar mass, is not as sensitive as the AKARI N3 image.

After deprojecting the N3 image to a face-on view, we performed median filtering with a box size of 25 pixels, corresponding to 36″ or 1.5 kpc, in order to remove the contribution from bright foreground stars and young stellar clusters in the M51a disk. Due to its high brightness, M51b was masked out. We then calculated an azimuthal average at each radius and subtracted it to remove axisymmetric components and thus to enhance the asymmetric spiral arm structure. The bright nucleus of M51a was also reasonably well removed from this procedure. After these preparation processes, we applied the wavelet analysis with Pet Hat function to extract components at 83″ (or 3.4 kpc) scale, which is found to best trace the M51a spiral structure (Dumas et al., 2011).

The central region with $r \leq 30''$ and the area within 75″ from the companion were excluded, and the maximum radius of the disk was set to be 240″. This arm and interarm definition is shown in the right panel of Figure 1. Pixels outside the defined area are excluded in the following analysis.

## 4. RESULTS

### 4.1. Color-Color Diagram

A map of the surface brightness ratio between two bands (i.e. color map) was created, using all the pixels five times brighter than the sky rms in both images. Here we discuss colors based on S11 (i.e. S7/S11, L15/S11, and L24/S11) only, since the S11 map shows the lowest arm/interarm contrast and thus is thought to best represent the total dust distribution.

Color-color diagrams, L15/S11 vs S7/S11 and L24/S11 vs S7/S11, are presented in the left panels of Figure 2. Data points are color-coded according to the region defined above. We find there are four points corresponding to the active nucleus that reside in a distinct area, while the other points for the center overlap with arm points.

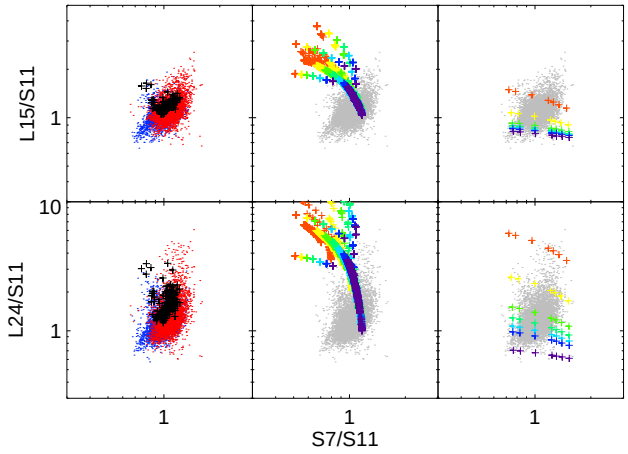


**Fig. 2.** Left: color-color diagrams of observational data, color coded by the defined regions. (Blue, red, black for interarm, arm, center, respectively.) Middle: model predictions from DL07 indicated by crosses with color coded by the PAH fraction. Right: model predictions from this work indicated by crosses color coded by the PAH fraction to large grains. (Both colors change from red to blue as the fraction increases.)

Differences between the arm and interarm are not significant. Nonetheless, a systematic variation of S7/S11, which is larger in the arms, is consistent with Sakon et al. (2007), who found a similar trend of the S7/S11 distribution in the nearby spiral galaxy NGC 6946.

### 4.2. Dust Models

We employed the interstellar dust model by Draine & Li (2007, hereafter DL07) and plotted a predicted color-color distribution superimposed on the observational data (middle panels of Figure 2. The color scheme represents the PAH mass fraction to the total dust $q_{\rm PAH}$, in the sense that it increases from red (0.47%) to blue (4.58%). The range of the other two variable parameters, the minimum threshold for radiation strength ($U_{\rm min}$) and the dust mass fraction exposed to $U_{\rm min} < U \leq U_{\rm max}$ ($\gamma$), was taken to be as wide as available: $\gamma$ =0–1 and $U_{\rm min} = 0.1$–$3 \times 10^5$. From these plots, it is clear that the observed color distribution is not fully covered by the combination of parameters available in DL07. They adopted a typical PAH ion-

ization fraction for the solar neighborhood ISM as a function of grain size. As a consequence, the profile of PAH band emission does not vary a lot according to the environments except in very strong radiation field, resulting in the very narrow range in predicted S7/S11 ratios.

Given the importance of variation of the PAH ionization state as discussed above, we decided to construct a new model including neutral and ionized PAHs and larger grains with their relative abundance being independently variable. Since we only have MIR data where the cold dust contribution is small, we used a gray body spectrum with $\beta = 2$ and $T = 100$ K to represent the flux from larger grains. Spectra for neutral and ionized PAHs were taken from DL07. Model predictions are plotted with the two free parameters, the relative strength of ionized PAH and gray body spectra to neutral PAH one (right panels of Figure 2. The symbol colors correspond to the fraction of neutral PAHs to larger grains, in the same sense as the middle panels. The dynamic range is a factor of 20 for both of the parameters. The S7/S11 distribution is now well explained by the variation of ionized/neutral PAH ratio.

## 5. DISCUSSION

From the comparison with observational data and DL07 models (Figure 2), we find that observational data points with L15/S11 $< 1$ and L24/S11 $< 1$ do exist while the models only predict these ratios larger than 1. In the following, we consider the contribution to the S11 flux from components other than interstellar dust, which could result in this discrepancy.

One possibility is the stellar continuum. We estimated its strength from the 2MASS $K_s$ image (Jarrett et al., 2003) assuming a black body spectrum with $T = 5,000$ K, and calculated its contribution to MIR bands. Since the stellar continuum monotonically decreases with wavelength at MIR regime while the observed in-band flux is rather flat, the estimated stellar contribution is $\sim 10\%$ in S7 and a few percent in S11.

Another candidate is gas emission lines. Dale et al. (2009) obtained MIR spectra from Spitzer/IRS toward selected positions in M51 (mostly star forming regions and nuclei) and measured the strength of these lines. Within the S11 spectral coverage, [Ne II] at $\lambda = 12.81$ $\mu$m is the strongest but its contribution to the S11 flux is estimated to be 3% at most.

Therefore, we conclude that the discrepancy of relative S11 brightness between observations and the DL07 model still remains unaccounted for.

Since the DL07 models with larger $q_{\rm PAH}$ tend to predict smaller values of L15/S11 and L24/S11 (middle panels of Figure 2, the S11 excess may indicate that in M51a $q_{\rm PAH}$ is larger than 4.58%, which is the largest value employed in their model. We here emphasize the importance of S11 data, which reveal the possibility of larger PAH fraction in M51a for the first time.

## REFERENCES

Arimatsu, K., et al., 2011, Characterization and Improvement of the Image Quality of the Data Taken with the Infrared Camera (IRC) Mid-Infrared Channels on Board AKARI, PASP, 123, 981

Dale, D. A., et al., 2009, The Spitzer Infrared Nearby Galaxies Survey: A High-Resolution Spectroscopy Anthology, ApJ, 693, 1821

Draine, B. T. & Li, A., 2007, Infrared Emission from Interstellar Dust. IV. The Silicate-Graphite-PAH Model in the Post-Spitzer Era, ApJ, 657, 810 (D07)

Dumas, G., Schinnerer, E., Tabatabaei, F. S., Beck, R., Velusamy, T., & Murphy, E., 2011, The Local Radio-IR Relation in M51, AJ, 141, 41

Feldmeier, J. J., Ciardullo, R., & Jacoby, G. H., 1997, Planetary Nebulae as Standard Candles. XI. Application to Spiral Galaxies, ApJ, 479, 231

Jarrett, T. H., Chester, T., Cutri, R., Schneider, S. E., & Huchra, J. P., 2003, The 2MASS Large Galaxy Atlas, AJ, 125, 525

Kaneda, H., Onaka, T., Suzuki, T., Takahashi, H., & Yamagishi, M., 2009, AKARI Observations of the ISM in Nearby Galaxies, ASP Conference Series, 418, 197

Murakami, H., et al., 2007, The Infrared Astronomical Mission AKARI, PASJ, 59, 369

Onaka, T., et al., 2007, The Infrared Camera (IRC) for AKARI – Design and Imaging Performance, PASJ, 59, 401

Sakon, I., et al., 2007, Properties of UIR Bands in NGC6946 Based on Mid-Infrared Imaging and Spectroscopy with Infrared Camera on Board AKARI, PASJ, 59, 483